Simulation of intermittent beam ion loss in a Tokamak Fusion Test Reactor experiment

Y. Todo[a)]

Theory and Computer Simulation Center, National Institute for Fusion Science, Toki 509-5292, Japan

H. L. Berk and B. N. Breizman

Institute for Fusion Studies, University of Texas at Austin, Austin, Texas 78712

Recurrent bursts of toroidicity-induced Alfvén eigenmodes (TAE) are studied using a self-consistent simulation model. Bursts of beam ion losses observed in the neutral beam injection experiment at the Tokamak Fusion Test Reactor [K. L. Wong *et al.*, Phys. Rev. Lett. **66**, 1874 (1991)] are reproduced using experimental parameters. It is found that synchronized TAE bursts take place at regular time intervals of 2.9 ms, which is close to the experimental value of 2.2 ms. The stored beam energy saturates at about 40% of that of the classical slowing down distribution. The stored beam energy drop associated with each burst has a modulation depth of 10%, which is also close to the inferred experimental value of 7%. Surface of section plots demonstrate that both the resonance overlap of different eigenmodes and the disappearance of KAM surfaces in phase space due to overlap of higher-order islands created by a single eigenmode lead to particle loss. Only co-injected beam ions build up to a significant stored energy even though their distribution is flattened in the plasma center. However, they are not directly lost, as their orbits extend beyond the outer plasma edge when the core plasma leans on a high field side limiter. The saturation amplitude is $\delta B/B \sim 2 \times 10^{-2}$, which is larger than would appear to be compatible with experiment. Physical arguments are presented for why the stored energetic particle response observed in the simulation is still plausible. © *2003 American Institute of Physics.* [DOI: 10.1063/1.1580122]

I. INTRODUCTION

The toroidicity-induced Alfvén eigenmode (TAE) (Ref. 1) can be destabilized by fast ions which have velocities comparable to the Alfvén velocity. A decade ago recurrent bursts of TAEs were observed with neutral beam injection (NBI) in the Tokamak Fusion Test Reactor (TFTR) (Ref. 2) and DIII-D (Ref. 3) experiments. Nearly synchronous with these TAE excitations, there were observed drops in neutron emission. Hence it was inferred that the TAE excitations caused a direct loss of the injected beam ions. In the experiments cited multiple TAE modes bursting at regular time intervals were observed. The modulation depth of the drop in neutron emission in the TFTR plasma was typically ∼10% (Fig. 4 of Ref. 2) and the beam confinement time is about one-half to one-third of the collisional slowing-down time.[4] This means that the TAE activity in these experiments substantially reduced the beam ion energy confinement time because TAE activity expels a substantial fraction of the energetic beam ions before this energy is absorbed by the core plasma through drag that is caused by classical collisions.

It was demonstrated in numerical simulations that used a reduced model employing a mapping method, that resonance overlap of multiple TAEs enhance the energy release from fast ions to TAEs and synchronizes the excitation of multiple TAEs.[5] For more quantitative comparisons with experiment,

more realistic simulations are needed. The entire geometry of a tokamak needs to be used together with a realistic TAE spatial dependence for determining the mode resonances. Candy *et al.*[6] carried out a reduced simulation with a realistic TAE spatial profile and where the linear eigenmodes were coupled to the beam ion dynamics. In the results of Ref. 6 a single dominant TAE grew to an amplitude of $\delta B/B \sim 2 \times 10^{-2}$ generating overlapping higher-order islands in phase space. The stochastic region created by the overlapping higher-order islands caused a complete flattening of the beam ion density. Another simulation method has been developed which is a Fokker–Planck-magnetohydrodynamic (MHD) simulation.[7] This simulation accelerated classical transport processes by using a shorter slowing-down time and a larger heating power than in experiment in order to perform the calculation in a reasonable computational time. This procedure leads to burst intervals that are shorter than experimental values by a factor of 1/4. Further in Ref. 7 it was reported that (a) a few percent of beam ions are lost with each TAE burst, (b) the unstable TAEs are excited in synchronism, and (c) the system hovers around a marginal stability state. However, the total stored beam energy was close to that of the classical distribution. Thus in the MHD simulation the TAE activity did not affect the stored beam energy although the beam ion spatial profile was greatly flattened compared to the classical distribution.

In this paper we report on an investigation, based on a reduced MHD method for a configuration typical of the

---

[a)]Electronic mail: todo@nifs.ac.jp

2888   © 2003 American Institute of Physics

Phys. Plasmas, Vol. 10, No. 7, July 2003

Simulation of intermittent beam ion loss . . .   2889

TFTR experiment, which had balanced beam injection.[2] The results of this simulation reproduce quite closely the following aspects of the experimental parameters; (a) synchronized bursts of multiple TAEs taking place at regular time intervals close to the experimental value; (b) a modulation depth in the stored energetic particles that is close to the one inferred in experiment; (c) stored beam energy that is about one-third of the classical slowing-down distribution. We also analyze the particle loss mechanism by constructing surface of section plots, and investigating the time evolution of purely co- and purely counter-injected beams to clarify the character of the response of the two types of beams.

II. SIMULATION MODEL

The simulation uses a perturbative approach where the TAE spatial profile is assumed fixed, while amplitudes and phases of the eigenmodes and the fast-ion nonlinear dynamics is followed self-consistently. For simplicity we consider concentric circular magnetic surfaces to describe the equilibrium magnetic field. We use as coordinates, the major radius R, the vertical coordinate z, the toroidal angle φ, the total speed V, and the pitch angle variable $\lambda \equiv V_\parallel / V$. The magnetic field is given by $\mathbf{B} = B_\varphi \hat{\varphi} + B_\vartheta \hat{\vartheta}$ with $B_\varphi = B_0 R_0 / R$, $B_\vartheta = -r B_0 / q(r) R$, where R is the local major radius, R_0 is the major radius on the magnetic axis, $q(r)$ is the safety factor, and ϑ is the poloidal angle with $\nabla \vartheta = \hat{\vartheta} / r$. The electromagnetic field is a superposition of this equilibrium field and the perturbed fields due to the TAE modes.

The fast-ion dynamics is followed using the guiding-center approximation with the particle velocity the sum of $\mathbf{E} \times \mathbf{B} / B^2$ ($\mathbf{u}_E$), grad-B ($\mathbf{u}_B$), curvature ($\mathbf{u}_C$) drifts, and the velocity parallel to the magnetic field lines. The guiding-center velocity is

$$V_{GC} = V \lambda \mathbf{b} + \mathbf{u}_E + \mathbf{u}_B + \mathbf{u}_C, \tag{1}$$

where $\mathbf{b}$ is the unit vector parallel to the magnetic field. For grad-B and curvature drifts only the dominant component due to the toroidal field is considered,

$$\mathbf{u}_B = \frac{m_f V^2 (1 - \lambda^2)}{2 q_f B_0 R_0} \hat{z}, \quad \mathbf{u}_C = \frac{m_f V^2 \lambda^2}{q_f B_0 R_0} \hat{z}. \tag{2}$$

The equation for the total speed is the sum of the interaction with the perpendicular electric field and drag from the background plasma,

$$\frac{dV}{dt} = \frac{q_f}{m_f V} (\mathbf{u}_B + \mathbf{u}_C) \cdot \mathbf{E}_\perp - \nu \left(V + \frac{V_c^3}{V^2} \right), \tag{3}$$

where ν is drag rate (inverse of the slowing-down time), and V_c is the critical velocity above which the energetic ion collisions with electrons dominate the slowing down process. The parallel electric field vanishes for the ideal magnetohydrodynamic (MHD) waves. The equation for the parallel velocity is given by (for example, see Ref. 8)

$$m_f V_\parallel \frac{dV_\parallel}{dt} = (V_\parallel \mathbf{b} + \mathbf{u}_C) \cdot (q_f \mathbf{E}_\perp - \mu \nabla B), \tag{4}$$

where μ is the magnetic moment. In Eq. (4) we consider only the toroidal field gradient for ∇B, which is consistent with the form for the grad-B and curvature drifts used in Eq. (2). Equations (3) and (4) give the equation for the pitch angle variable

$$\frac{d\lambda}{dt} = \frac{(\lambda - \lambda^3)}{2 B_0 R_0} E_z + \frac{V(1 - \lambda^2)}{2R} b_R. \tag{5}$$

A fourth-order Runge–Kutta method is employed to integrate these particle orbit equations. Pitch angle scattering is taken into account at the end of each time step by using a Monte Carlo procedure,[9] where a particle's pitch angle is altered according to the relation

$$\lambda_{\text{new}} = \lambda_{\text{old}} (1 - 2 \nu_d \Delta t) \pm [(1 - \lambda_{\text{old}}^2) 2 \nu_d \Delta t]^{1/2}, \tag{6}$$

where ν_d is the pitch angle scattering rate, and $\pm$ denotes a randomly chosen sign with equal probability for plus and minus.

The algorithm to advance the amplitude and phase of TAE mode is similar to the one developed in Refs. 5 and 10. For a single eigenmode with toroidal mode number n and real frequency ω, the scalar potential Φ and the parallel vector potential $A_\parallel$ are given by

$$\Phi_s(R, \varphi, z) = X \sum_m \phi_m(r) \sin(n\varphi + m\vartheta - \omega t), \tag{7}$$

$$\Phi_c(R, \varphi, z) = Y \sum_m \phi_m(r) \cos(n\varphi + m\vartheta - \omega t), \tag{8}$$

$$\Phi = \Phi_s + \Phi_c, \tag{9}$$

$$A_{\parallel s}(R, \varphi, z) = X \sum_m a_{\parallel m}(r) \sin(n\varphi + m\vartheta - \omega t), \tag{10}$$

$$A_{\parallel c}(R, \varphi, z) = Y \sum_m a_{\parallel m}(r) \cos(n\varphi + m\vartheta - \omega t), \tag{11}$$

$$A_\parallel = A_{\parallel s} + A_{\parallel c}, \tag{12}$$

where a relation $a_{\parallel m} = \phi_m (n - m/q) / \omega R_0$ is satisfied since the parallel electric field vanishes for the ideal MHD waves, and X and Y denote the amplitude of sine and cosine part, respectively. The electromagnetic field of the eigenmodes are determined from the potentials,

$$\mathbf{E}_{s(c)} = -\nabla_\perp \Phi_{s(c)}, \tag{13}$$

$$\mathbf{B}_{s(c)} = \nabla_\perp \times (A_{\parallel s(c)} \mathbf{b}). \tag{14}$$

The time evolution of the amplitude X and Y are

$$\frac{dX}{dt} = [-\langle \mathbf{j}_f \cdot \mathbf{E}_s \rangle / 2 W_s - \gamma_d] X, \tag{15}$$

$$\frac{dY}{dt} = [-\langle \mathbf{j}_f \cdot \mathbf{E}_c \rangle / 2 W_c - \gamma_d] Y, \tag{16}$$

$$\mathbf{j}_f = \sum_i w_i \frac{m_f V_i^2 (1 + \lambda_i^2)}{2 B_0 R_0} \hat{z}, \tag{17}$$

$$W_{s(c)} = \left\langle \frac{1}{2\mu_0} \mathbf{B}_{s(c)}^2 + \frac{1}{2\mu_0 V_A^2} \mathbf{E}_{s(c)}^2 \right\rangle, \qquad (18)$$

where γ_d is the intrinsic mode damping rate, $\mathbf{j}_f$ is the sum of each particles' grad-B and curvature drift current, w_i is a weight of the ith beam particle, W_s and W_c are the mode energy for the sine part and cosine parts of the perturbed field amplitude, and $\langle \ \rangle$ denotes volume average.

The code is benchmarked with respect to the linear growth rate of the alpha-particle-driven $n=4$ TAE in the TFTR D-T plasma shot #103101.[11] The eigenmode equations [e.g., Eqs. (3) and (4) of Ref. 12] for two poloidal harmonics $m=6$ and $m=7$ are solved to obtain the $n=4$ TAE structure. The initial energetic particle distribution is similar to that of a previous particle simulation reported in Ref. 10, where roughly an isotropic distribution for the energetic particles (which in this benchmark case were alpha particles) is used in the velocity space. In this benchmark test, which uses 4.2×10^6 markers to represent energetic particles, the collisions are neglected because they do not affect the linear growth rate. The linear growth rate obtained from this simulation, is 1.0×10^{-2} of the mode frequency. This linear growth rate is close to what is observed in the previous particle simulation 1.1×10^{-2} (Ref. 10) and calculated in the NOVA-K code 8×10^{-3}.[13] The discrepancy might be due to the simplified flux surfaces used here, which are idealized to be concentric. For this benchmark case and for the TAE burst simulation, which is reported in the next section, a standard "full-f" method is employed. With the full-f method it is easy to account for the particle source and sink, especially in allowing for the removal of particles that reach the wall. Such removal in a δf algorithm[14] would introduce technical difficulties in implementation. The particle source (beam ion injection) and sink (beam ion loss) are essential ingredients for the establishment of the TAE bursts.
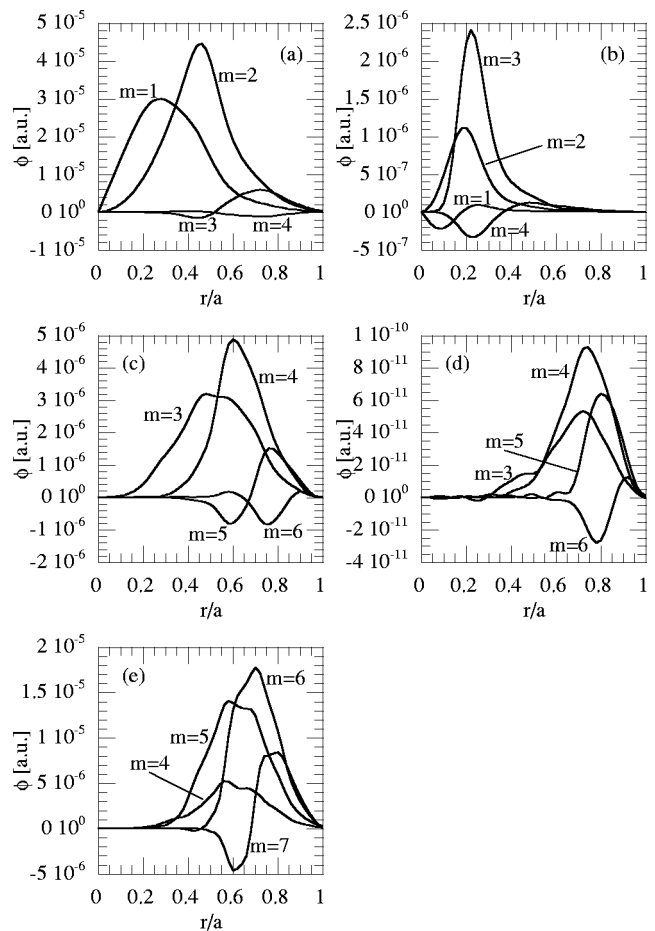

FIG. 1. Major four harmonics of the electric potential of Alfvén eigenmodes with the toroidal mode number of (a) $n=1$, $\omega=0.283\omega_A$ (mode 1), (b) $n=2$, $\omega=0.404\omega_A$ (mode 2), (c) $n=2$, $\omega=0.278\omega_A$ (mode 3), (d) $n=2$, $\omega=0.257\omega_A$ (mode 4), and (e) $n=3$, $\omega=0.330\omega_A$ (mode 5), where $\omega_A \equiv V_A/R_0 = 1.35\times10^6$ s^{-1}.

III. TAE BURSTS

A. Simulation results

For the TAE burst simulation the q-profile is taken to vary quadratically with minor radius from a central value of 1.2 to an edge value of 3.0, $q(r)=1.2+1.8(r/a)^2$. In the "vacuum" region the q-profile is modeled with a simplified form of $q(r)=3(r/a)^2$. The major and minor radii are $R_0 = 2.4$ m and $a=0.75$ m. The magnetic field is 1.0 T on axis. The spatial structure and the real frequency of the eigenmodes are obtained from a Fokker–Planck-MHD simulation.[7] The plasma density in the simulation is chosen for simplicity to be uniform 2.2×10^{19} m^{-3}. Both the core plasma ions and the beam ions are deuterium. Five eigenmodes are taken into account. Their toroidal mode number and real frequency are, respectively, (a) $n=1$, $\omega=0.283\omega_A$ (mode 1), (b) $n=2$, $\omega=0.404\omega_A$ (mode 2), (c) $n=2$, $\omega=0.278\omega_A$ (mode 3), (d) $n=2$, $\omega=0.257\omega_A$ (mode 4), and (e) $n=3$, $\omega=0.330\omega_A$ (mode 5), where $\omega_A \equiv V_A/R_0 = 1.35\times10^6$ s^{-1}. The spatial profile of the eigenmodes is shown in Fig. 1. The linear damping rate of each mode is assumed to be constant at 4×10^3 s^{-1}. The Fokker–Planck-MHD simulation does not give the part of the mode damping rate which

depends on the kinetic properties of the bulk plasma. This leads to an arbitrariness in the choice of the damping rate and the eigenmodes in the present simulation. We have chosen the aforementioned set of eigenmodes and damping rates that roughly reproduces the experimental results. Even if eigenmodes and damping rates in the experiment are somewhat different from those in the simulation, we still expect that the major results obtained in this work, such as the particle loss mechanism and the difference between co- and counter-injected beams, will correlate well with the experiment. We carried out runs with different damping rates. With a damping rate of 3×10^3 s^{-1} the major results are essentially the same as the run reported in this paper. The saturation level of the stored beam energy is lower by about 20% and the burst intervals are shorter by about 10%. However, at a lower damping rate a different type of response is possible. Indeed for a damping rate of 2×10^3 s^{-1}, the observed bursty pattern changes and we obtain a response that is more steady but with anomalous particle loss.

Beam ions have balanced injection with a constant heating power of 10 MW and with a spatial Gaussian profile whose radial scale length is 0.3 m. The injection energy is 110 keV which roughly corresponds to the Alfvén velocity

Phys. Plasmas, Vol. 10, No. 7, July 2003

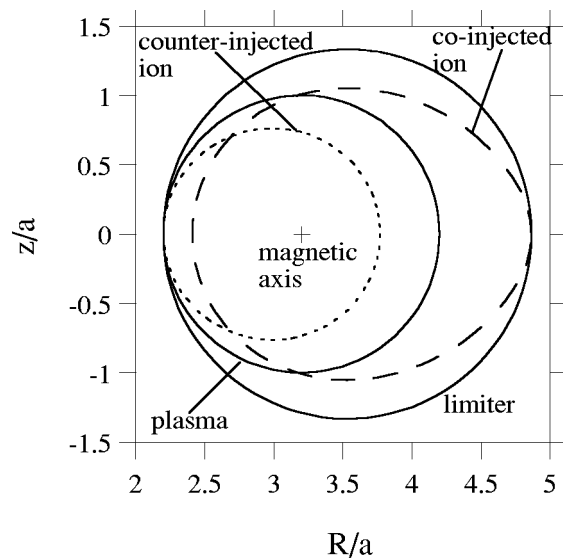Simulation of intermittent beam ion loss . . .   2891

FIG. 2. Configuration of the plasma and the limiter, and examples of counter-injected beam ion orbit and co-injected beam ion orbit. The velocity of the co-injected ion is parallel to the plasma current. The orbits of co-injected (counter-injected) beam ions are displaced from magnetic surfaces towards the weak (strong) field side.
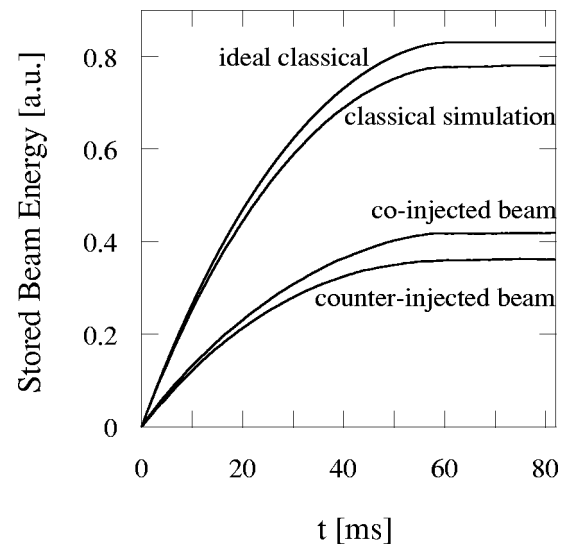

FIG. 3. Time evolution of stored beam energy of an ideal classical distribution where there is no direct edge loss with that of a classical simulation where there is edge loss due to prompt losses and pitch angle scattering. Also shown for the latter case is the time evolution of the separate co- and counter-injected beams.

parallel to the magnetic field. The injected beam ion has a uniform pitch angle distribution in the range of $0.7 \leq |\lambda| \leq 1$. In the TFTR experiment two types of limiters, toroidal belt limiter and three poloidal limiters, were used. In the poloidal cross section the limiters roughly defined a circle of radius 1 m. We model these limiters by removing particles if they reach a torus with axis at $R/a = 3.53$ ($R = 2.65$ m) on the midplane and minor radius $1.33a$ (1 m). Figure 2 shows the configuration of the plasma and the limiter where particles are removed. Thus the plasma is leaning on the limiter at the strong field side, while at the weak field side there is a space from the plasma edge to the limiter whose width is $0.67a$ (0.5 m). In addition to the plasma and the limiter, examples of counter-injected beam ion orbit and co-injected beam ion orbit are shown in Fig. 2. By convention the velocity of a co-injected ion is parallel to the plasma current and in our case the velocity is parallel to the toroidal magnetic field as well. Thus negative values of λ correspond to the counter-injected beam ions and positive values of λ correspond to co-injected beam ions. The injected particle speed is $V = V_0$. The orbits of co-injected (counter-injected) beam ions first encounter the plasma edge on the weak (strong) field side independent of the direction of the toroidal magnetic field. Note that the co-injected particles can stick out of the plasma on the weak field side, whereas the counter-injected particles are immediately removed by the limiter when they reach the edge of the strong field side.

The slowing-down time is assumed to be 100 ms. For an experimental electron temperature of 2 keV the critical energy, above which the collisions with electrons dominate the slowing down process, is 37 keV. The pitch angle scattering rate is given by $\nu_d = \nu V_c^3 / 2V^3$. Because the pitch angle scattering rate diverges as the particle speed reaches zero, we remove particles when they reach $V = 0.1V_0$. In order to see the effect of beam ion confinement from prompt loss, pitch-

angle scattering, and the numerical sink at $V = 0.1V_0$, we carry out a simulation with 5.2×10^5 particles without any TAEs. In Fig. 3 we show the time evolution of the stored beam energy and compare it with that of an ideal classical distribution which is established with only a particle source and slowing down without any of the particle sinks mentioned above. In the relative units of this figure, the ideal classical distribution saturates at relative level of 0.83, whereas that of the simulation saturates at a relative level of 0.78, namely, 94% of that of the ideal classical distribution. Thus the induced particle loss due to prompt loss, pitch-angle scattering, and the numerical sink are small. Both the ideal classical distribution and simulation have saturated at $t = 60.3$ ms when the injected particles slow down to $V = 0.1V_0$. This suggests that the effects of the numerical sink at $V = 0.1V_0$ are negligible. We have carried out another classical simulation without any pitch angle scattering for the purpose of investigating whether the cause of classical particle loss is due to prompt loss or pitch-angle scattering. The relative saturation level without the pitch angle scattering is 0.79 which is close to that obtained by including pitch angle scattering, which gives a relative saturation level of 0.78. Thus the particle loss to the walls in the classical simulation is due primarily to the prompt loss of counter-injected beam particles with virtually no prompt loss of for co-injected beam particles.

The number of particles used in the simulation runs to be described below is 2.1×10^6 (unless otherwise specified). We start the simulation at an initial time taken as $t = 0$ when the beam ions are first injected. As time passes, energetic ions gradually accumulate. The time evolution of the amplitude of each mode is shown in Fig. 4. We see that synchronized bursts take place recurrently at a burst interval that is roughly 2.9 ms which is reasonably close to that of the experimental value of 2.2 ms in the TFTR experiment that we are compar-
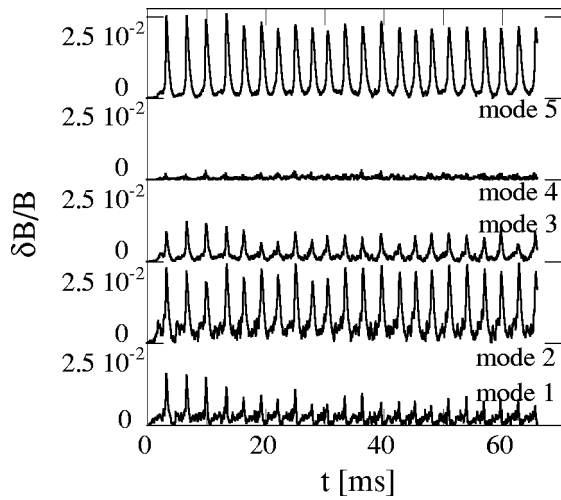
FIG. 4. Amplitude evolution of all the eigenmodes during the simulation.

ing with. Figure 5 shows the time evolution of the dominant two modes 2 and 5, and density at various minor radii. We can see that the mode 2, which is located at the plasma center, has precursory growth before both the modes grow together in synchronism during each burst. Because the beam injection profile peaks at the plasma center, mode 2 is destabilized before mode 5. We can see complete flattening of the density at the plasma core ($r/a < 0.72$) and small increase in
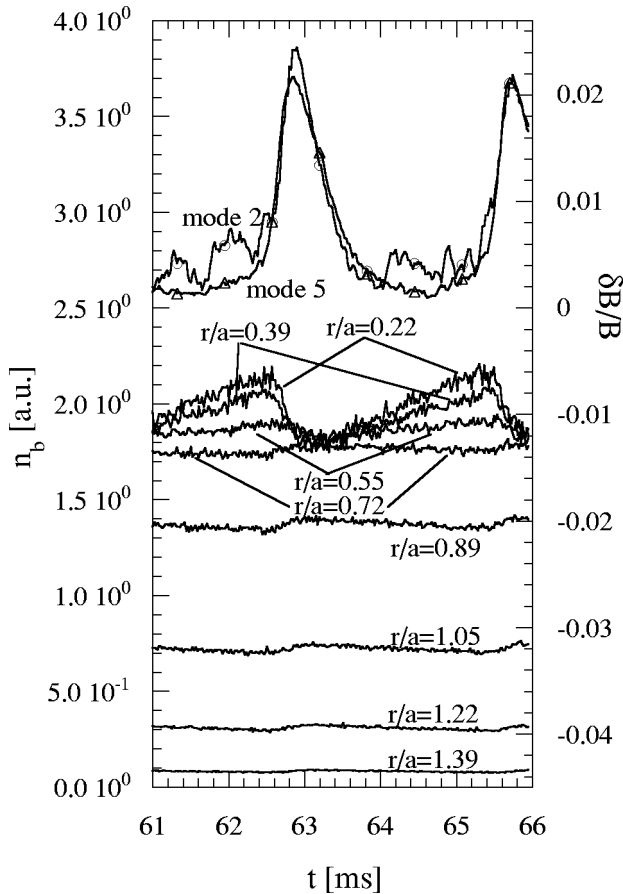
FIG. 5. Time evolution of the dominant two modes 2 and 5 and the density of the co-injected beam ions at various minor radii.
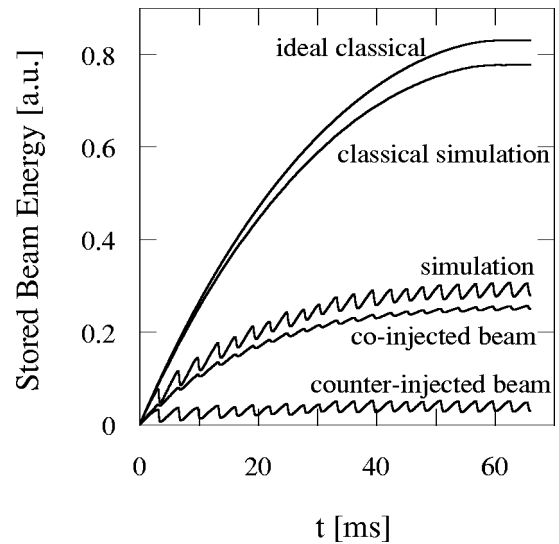
FIG. 6. Time evolution of the stored beam energy from the combined effect of classical transport and self-consistent TAE mode excitation. For comparison the stored energy of the "ideal classical distribution" and the "classical simulation" results are shown.

the density at the plasma edge ($r/a \geqslant 0.72$). The beam ions stored at the plasma core during the quiescent phases are transported to the plasma edge and lost during the bursts. In Fig. 6 we show the time evolution of the stored beam energy and compare it with that of the two classical distributions mentioned above. The modulation depth of the drop in the stored beam energy is 10% which is close to the inferred experimental value of 7%. In the relative units of this figure, the distribution that would result without fluctuations (the "classical simulation" in Fig. 6), saturates at a relative level of 0.78, whereas that of the simulation with TAE bursts saturates at 40% of this value, at a relative level of 0.31 and with a volume averaged beam ion beta value (defined here as 2/3 of stored kinetic energy divided by the magnetic field energy averaged over the volume) of 0.6%. We thereby find good agreement between the simulation and the experiment where the beam ion energy confinement time is about one-half to one-third of the beam energy slowing down time and the estimated beam ion beta value is 0.5%.[2,4]

A basic feature of the simulation that is apparent in Fig. 6 is the dramatic difference between the stored beam energy of co- and counter-injected beams whose velocity is parallel and antiparallel to the plasma current, respectively. The loss in counter-injected beam energy induced by the TAEs' activity is 88%, while that in co-injected beam energy is 37%. Figure 7 shows the spatial beta profiles of both co- and counter-injected beams at the end of the simulation. The beta profile of the co-injected beam ions is broadened and extended beyond the plasma edge ($r/a = 1$), while that of the counter-injected beam sharply peaks at the plasma center. Figure 8 shows a plot of the time evolution of the counter-injected and co-injected beam ion density as functions of the minor radius r after they are averaged in the poloidal and toroidal directions. We see substantial drops in density at the plasma center both for the counter-injected and the co-injected beam ions at each burst. At the plasma edge small
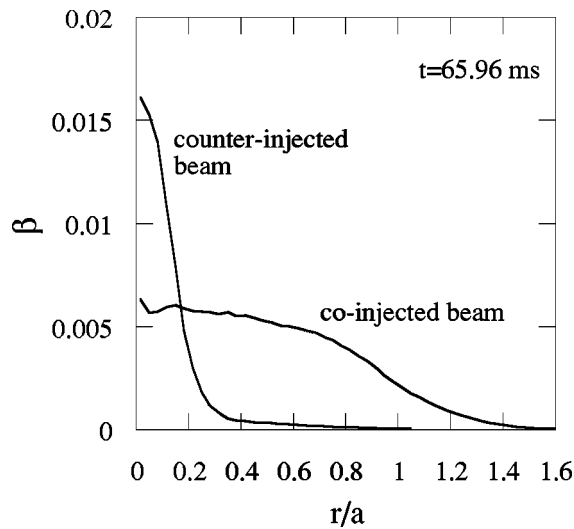
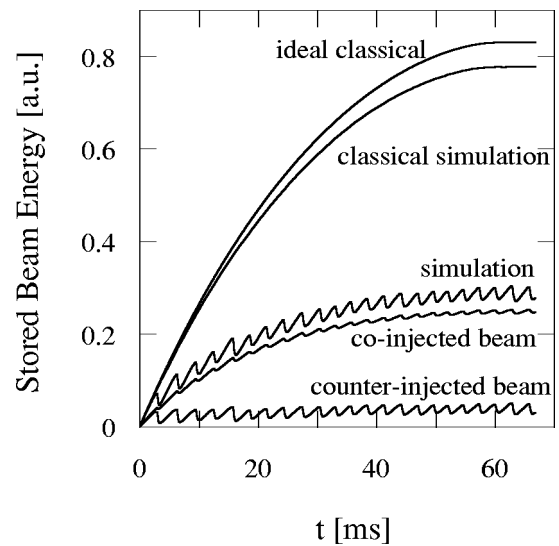FIG. 7. Radial beta profiles at the end of the simulation that develop from co- and counter-injected beams.

FIG. 9. Time evolution of stored beam energy using 5.2×10^5 particles, a quarter of the standard run (shown in Fig. 6). The correlation between the results of the two runs indicate numerical convergence.

increases in density can be seen as ridges in Fig. 8(b). In Sec. III C we will investigate the particle loss mechanism and discuss why the stored beam energy is so different between the co- and counter-injected beam ions.

FIG. 8. (Color) Evolution of beam ion density in (t,r) space (after $t = 50$ ms) for: (a) counter-injected beam ions; (b) co-injected beam ions.

B. Convergence with particle number

To check numerical convergence a test run was carried out where the number of particles was chosen as 5.2×10^5. This was a quarter of the standard number of particles 2.1×10^6 that was used in the previous run. The results of the test run are shown in Fig. 9 where we display the time evolution of the stored beam energy and compare it with that of the two classical distributions. We see that synchronized bursts take place recurrently at a burst interval 2.8 ms which is close to the value of 2.9 ms for the run that uses the standard number of particles. The modulation depth of the drop in the stored beam energy in the test run is 9% (10% with the standard number of particles). In the relative units of this figure the stored beam energy of the test run saturates at a relative level of 0.30 (0.31 with the standard number of particles). We conclude that we have a good numerical convergence so that the number of particles used is sufficient for the results presented in this work.

C. Particle loss mechanism

We now consider how the energetic particle loss mechanism is to be understood. To study this, we study surface of section plots where only one eigenmode is taken into account and the amplitude of the eigenmode is at a constant value. We choose particles which have a constant value of $E' \equiv E - \omega P_\varphi / n$, where E is particle energy and P_φ is canonical toroidal momentum, because E' is conserved in the interaction of a constant amplitude wave with frequency ω and toroidal mode number n. Then with a single mode we have a conserved variable and we can make surface of section plots that are easily interpretable (otherwise, with more than one mode we would obtain phase oscillations about KAM surfaces that ruin the simplicity of the output so that we would have difficulty resolving KAM boundaries). Thus by looking at a set of single-mode results we can predict the emergence of stochasticity, and whether stochastic regions (or phase
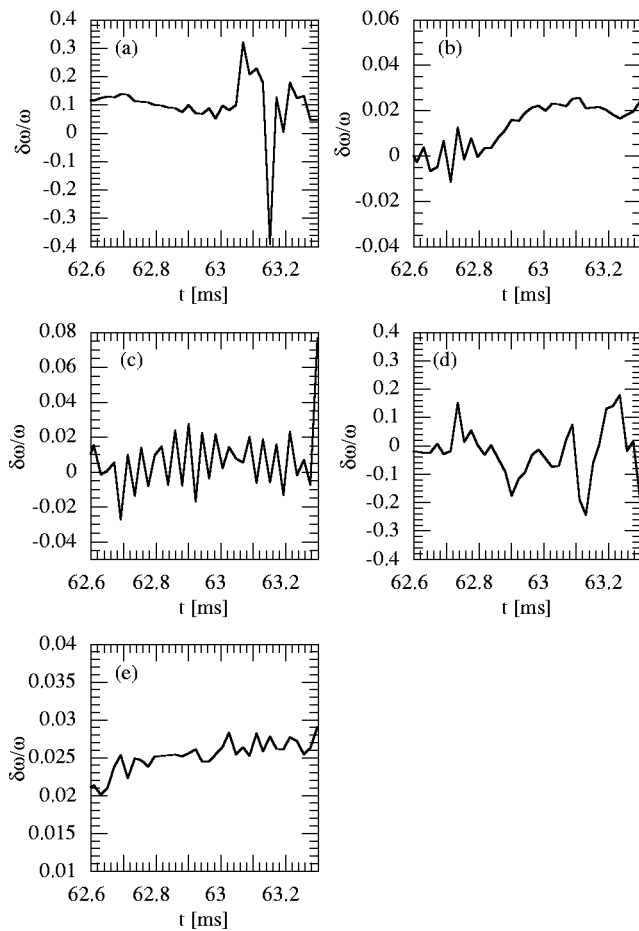
FIG. 10. Time evolution of frequency modulation during a pulsation in the standard run of (a) mode 1, (b) mode 2, (c) mode 3, (d) mode 4, and (e) mode 5.
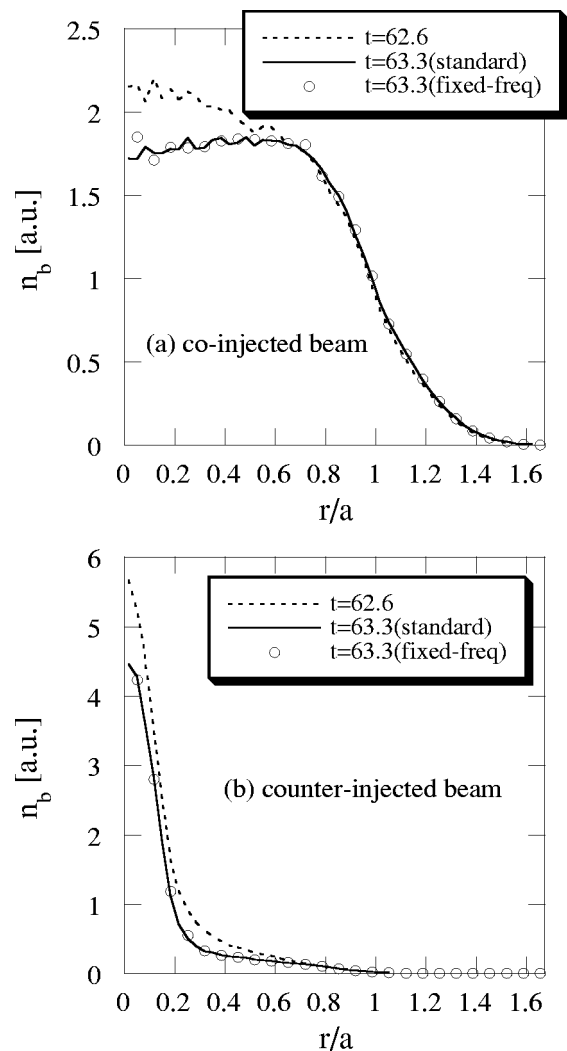

FIG. 11. Comparison of radial density profiles of a test particle run (circles) with a standard simulation run (solid curve). An identical initial profile is taken at $t=62.6$ ms (dashed curve) for (a) co-injected beam and (b) counter-injected beam. In the test particle run the amplitudes of all the modes follow the time history of the standard run but frequencies are clamped at the linear eigenfrequency of each mode.

space islands) from different plots overlap each other. We can thereby determine whether we have achieved global stochasticity. Because the co-passing (counter-passing) particles are lost at the outer (inner) edge, we choose a separate E' for co- and counter-passing particles. Hence for co-passing particles E' is defined on the outer edge midplane at $R/a=4.87$, with $V=V_0$, and $\lambda=1$, while for counter-passing particles E' is defined on the inner edge at $R/a=2.2$, with $V=V_0$, and $\lambda=-1$. In this surface of section plots the speed of particles varies from the plasma center to the limiter. The largest difference in the speed is 30% for co-passing particles with mode 1, for which the toroidal mode number is $n=1$, while the smallest difference is 6% for counter-passing particles with mode 5, for which the toroidal mode number is $n=3$. In the surface of section plot we print the major radius R/a and phase, $n\varphi-\omega t$, of a counter- (co-) passing particle each time the poloidal angle of the particle reaches $\theta=180°$ (0°). Note that in these plots the co-passing particles can reach radii that stick out of the plasma.

Before we report the surface of section plots, it must be ascertained whether the mode frequency remains roughly constant during a pulsation period of the simulation. In Fig. 5 we can see that the particle transport takes place from $t=62.6$ ms to $t=63.3$ ms during a pulse. We investigate how much the mode frequencies change during this period and

the results are shown in Fig. 10. The frequencies of modes 2 and 5, which have the largest amplitudes, change by about 3% and 1% for each eigenfrequency. The frequency fluctuations of the other modes are larger, because the frequency of small amplitude modes are more strongly affected by numerical noise due to the discreteness arising from using a finite number of particles. To investigate the effect of the frequency change on the particle transport we carried out a test particle run which starts with the data of the standard run at $t=62.6$ ms. In this test particle run the amplitudes of all the modes evolve by following the time history of the standard run but their frequencies are fixed at the linear eigenfrequency of each mode. In Fig. 11 we compare the density profiles at $t=63.3$ ms with those of the standard run. We see good agreements between the two runs. Thus, the effect of the mode frequency change is negligible with regard to particle transport and the use of the surface of section plots (described below) is relevant to the understanding of the particle loss mechanism.
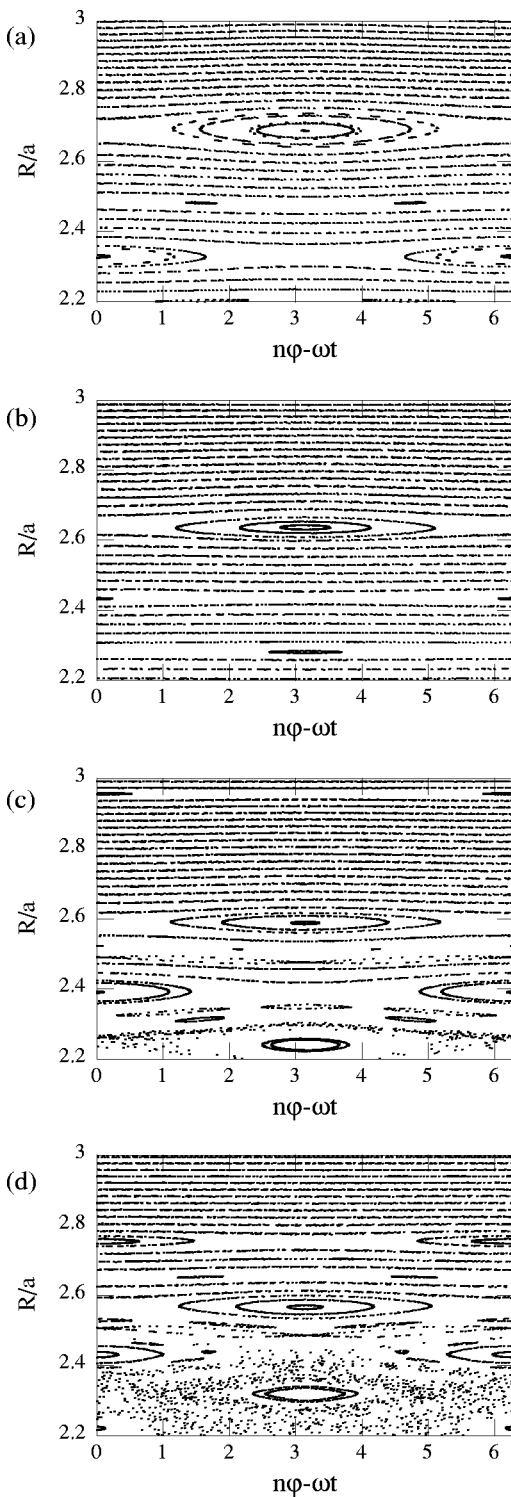
FIG. 12. Surface of section plots for counter-injected beam ions where the field amplitude is fixed in time at an ambient level $\delta B/B = 2 \times 10^{-3}$ for (a) mode 1, (b) mode 2, (c) mode 3, and (d) mode 5.
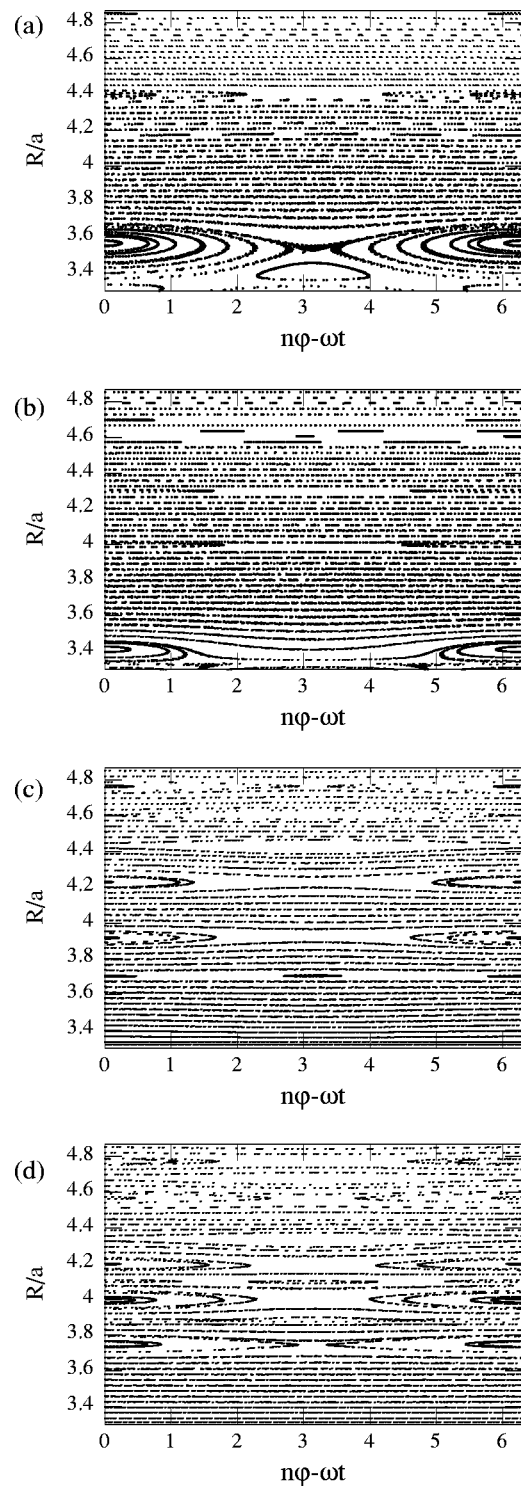
FIG. 13. Surface of section plots for co-injected beam ions for the same mode and amplitude as Fig. 12.

Let us start with investigating the ambient amplitudes between bursts. We show in Figs. 12 and 13 surface of section plots for the counter-passing and co-passing particles, respectively, where the field amplitude of the dominant four eigenmodes is fixed in time at an ambient level $\delta B/B = 2 \times 10^{-3}$. Figure 12 shows the plots for the strong field side, while Fig. 13 is for the weak field side. We see in Fig. 12(d)

that KAM surfaces disappear near the plasma edge $R/a < 2.4$. Thus even with the ambient amplitude particle loss takes place but the amount of loss is too small to stop the increase in the stored beam energy because only the counter-passing particles at $R/a < 2.4$ are lost. Figure 14 shows surface of section plots for the counter-passing particles at $2.2 < R/a < 2.6$ where the field amplitude of mode 5 is fixed at a lower level $\delta B/B = 8 \times 10^{-4}$. Now the particle dynamics
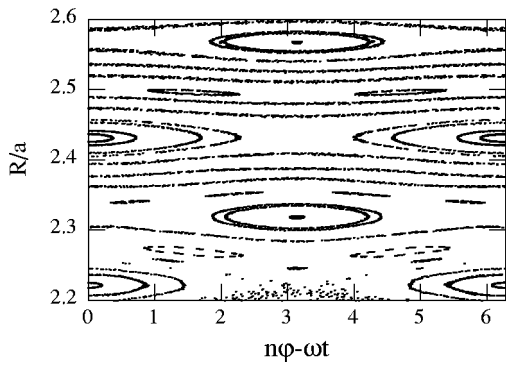
FIG. 14. Surface of section plots for counter-injected beam ions for mode 5 with lower amplitude $\delta B/B = 8 \times 10^{-4}$.

hardly have any region of stochasticity. Instead, we see the emergence of second- and fourth-order islands around $R/a = 2.27$ and $R/a = 2.35$, respectively, in addition to the two first-order islands around $R/a = 2.22$ and $R/a = 2.32$. With increasing field amplitude these islands overlap to eventually destroy the KAM surfaces and create the stochastic region that appears in Fig. 12(d).

Next, we examine the field amplitude when the loss stops the increase in the stored beam energy. The markers in Fig. 15 show the mode amplitude at the times when the stored beam energy takes on relative maximum values during the simulation run. We show in Figs. 16 and 17 the surface of section plots for the counter-passing and co-passing particles, respectively, where the field amplitude of the largest four eigenmodes is fixed in time at (a) $\delta B/B = 4 \times 10^{-3}$ for mode 1, (b) $\delta B/B = 7 \times 10^{-3}$ for mode 2, (c) $\delta B/B = 4 \times 10^{-3}$ for mode 3, and (d) $\delta B/B = 6 \times 10^{-3}$ for mode 5. These amplitudes are higher than the ambient amplitudes between bursts, but considerably lower than the peak amplitudes these bursts reach. We see in Figs. 16(d) and 17(d) that the KAM surfaces are destroyed for mode 5 near the plasma edge $R/a < 2.6$ and $R/a > 4.6$, respectively, which then leads to particle loss even before the modes reach their peak amplitude. We should notice that in Fig. 17(d) the KAM surfaces exist at $4.4 < R/a$
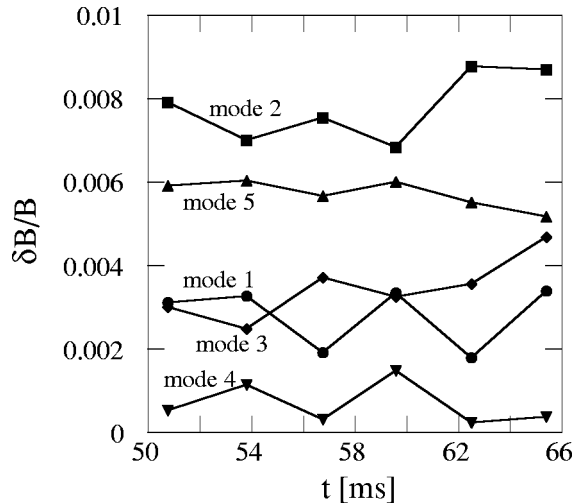

FIG. 15. Amplitude of all the eigenmodes at the times when the value of the stored beam energy reach relative maxima.
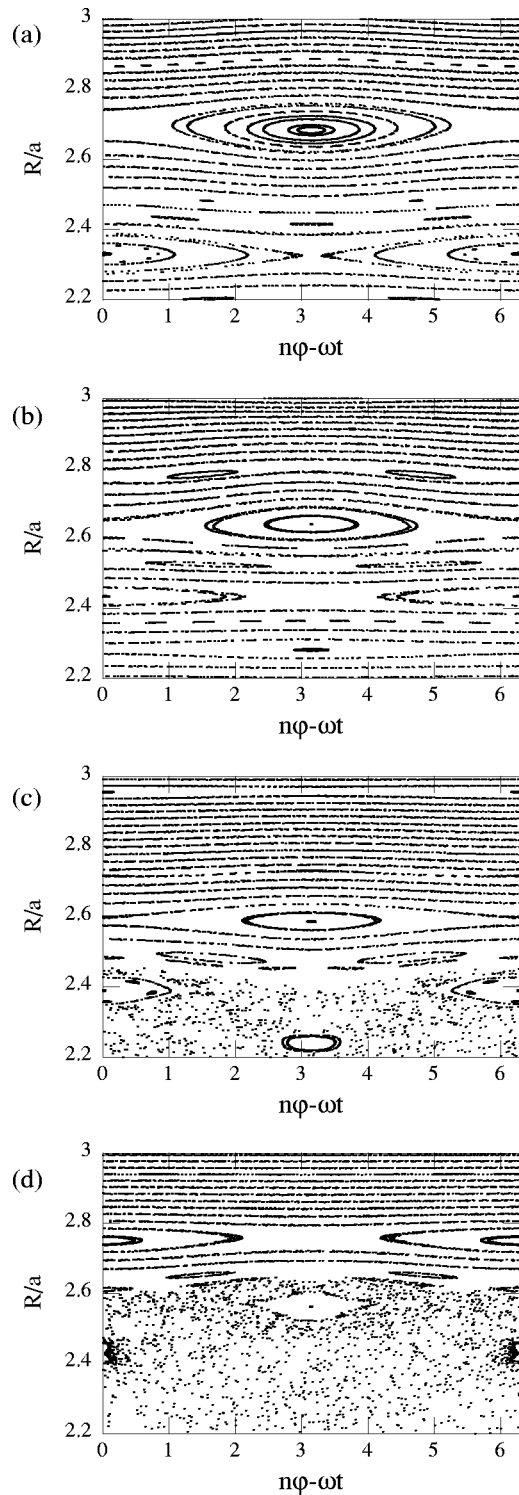

FIG. 16. Surface of section plots for counter-injected beam ions when the field amplitude is fixed in time at: (a) $\delta B/B = 4 \times 10^{-3}$ for mode 1, (b) $\delta B/B = 7 \times 10^{-3}$ for mode 2, (c) $\delta B/B = 4 \times 10^{-3}$ for mode 3, and (d) $\delta B/B = 6 \times 10^{-3}$ for mode 5.

< 4.6 for co-injected beam ions, which strongly inhibit co-particle diffusion from the plasma center to the edge at this field amplitude. Thus there is a substantial delay in co-moving particle loss compared with that from counter-moving particles.

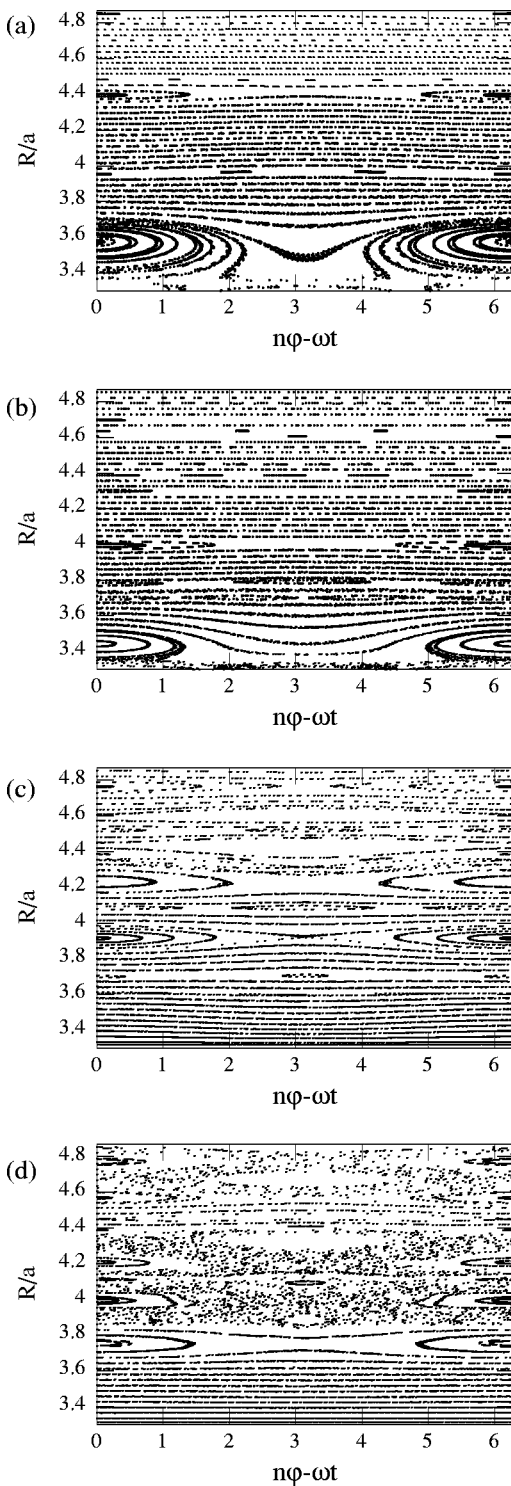In Figs. 18 and 19 we show surface of section plots at

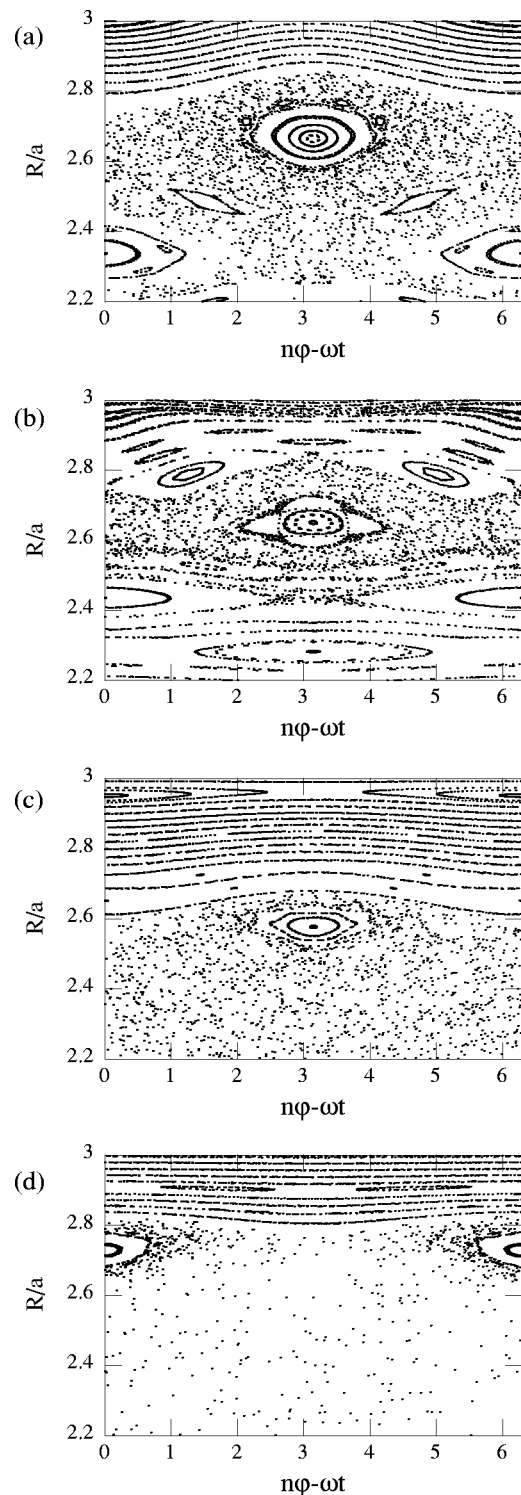FIG. 17. Surface of section plots for co-injected beam ions for the same mode and amplitude as Fig. 16.

FIG. 18. Surface of section plots for counter-injected beam ions with saturation amplitudes; (a) mode 1, $\delta B/B=1.5\times10^{-2}$, (b) mode 2, $\delta B/B=2.2\times10^{-2}$, (c) mode 3, $\delta B/B=1.2\times10^{-2}$, and (d) mode 5, $\delta B/B=2.5\times10^{-2}$.

the saturation amplitude of the largest four eigenmodes for counter- and co-injected beam ions, respectively, with saturation amplitudes (a) $\delta B/B=1.5\times10^{-2}$ for mode 1, (b) $\delta B/B=2.2\times10^{-2}$ for mode 2, (c) $\delta B/B=1.2\times10^{-2}$ for mode 3, and (d) $\delta B/B=2.5\times10^{-2}$ for mode 5. The KAM surfaces are destroyed near the limiter [$R/a=2.2$ in Figs. 18(a), 18(c), 18(d), and at $R/a=4.87$ in Figs. 19(c), 19(d)]. Thus the potential for particle loss appears to be very similar

for both counter- and co-injected beam ions at the highest saturation amplitudes. There is however a significant difference in the stored beam energy between counter- and co-injected beam ions. It can arise from the difference in the particle diffusion time. We have found two qualitative reasons for this. First, the unperturbed orbits of co (counter)-
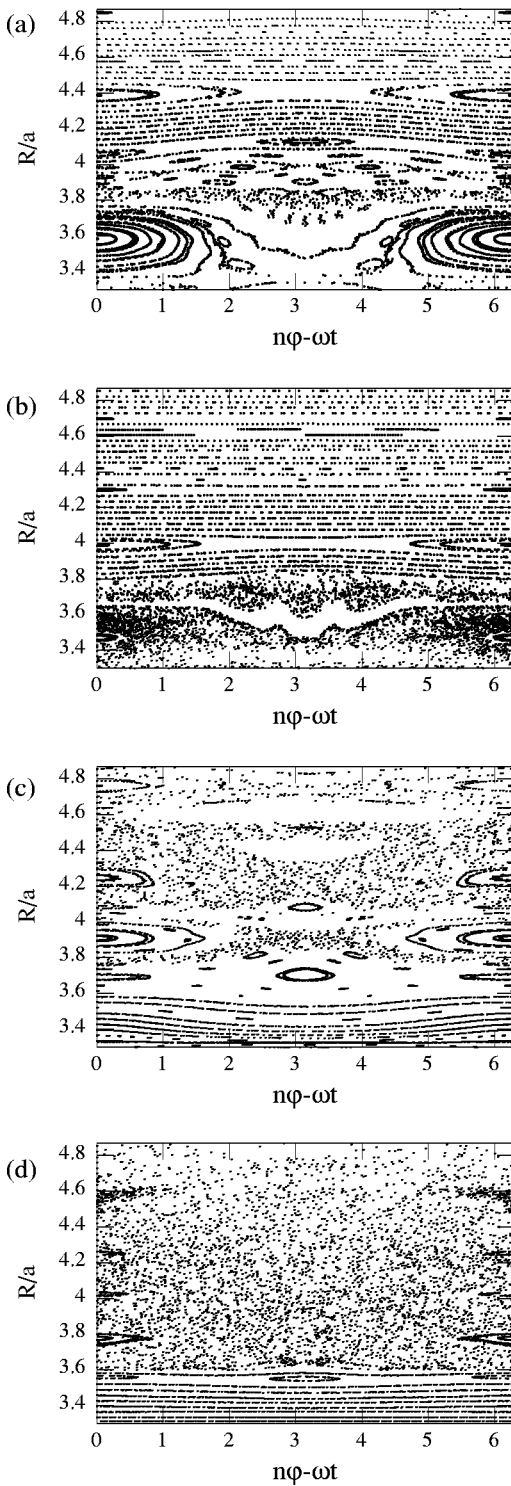
(a)

(b)

(c)

(d)

FIG. 19. Surface of section plots for co-injected beam ions for the same mode and amplitude as Fig. 18.
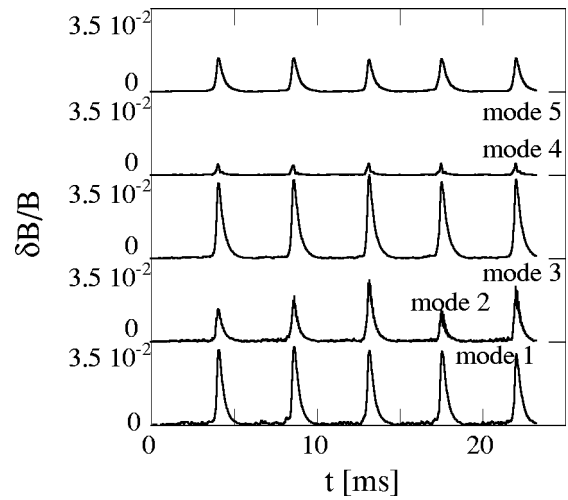

FIG. 20. Amplitude evolutions of all the eigenmodes for counter-injection.

turbed fields within the plasma. Further co-passing particles have room to move to larger radial distance than counter-passing particles. Thus for fixed perturbing fields, these aspects would increase the diffusion time of co-injected beam ions compared to that of the counter-injected beam ions. Second, as mentioned above, the KAM surfaces at $4.4 < R/a < 4.6$ for co-injected beam ions in Fig. 17(d) suppress the transport in the outer region for a large fraction of the TAE burst time. Apparently, the time that the co-passing particles are diffusive is short enough to prevent loss of a large fraction of the stored co-passing particle energy. On the other hand for counter-injected beam ions tend to be rapidly lost. The exception is near the plasma center where it can be observed in Fig. 18 that KAM surfaces still exist which leads to the peaked central density profile of the counter-injected particles.

injected beam ions are displaced from magnetic surfaces towards the weak (strong) field side. It is significant that on the weak field side there is a spatial region (where there are no perturbed fields) which extends from the plasma edge to the limiter as shown in Fig. 2. Thus the time-averaged displacement of co-passing particles that are sticking out of the plasma and its resulting diffusion coefficient is smaller than for counter passing particles which always sample the per-
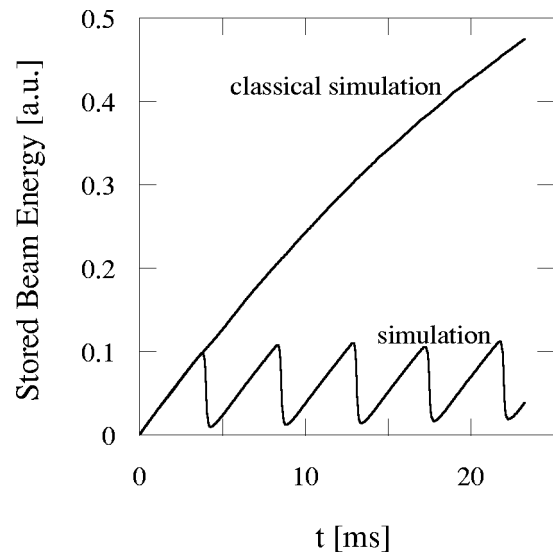

FIG. 21. Time evolution of stored beam energy using only counter-injected beams. Result from simulation is compared with the classical result.

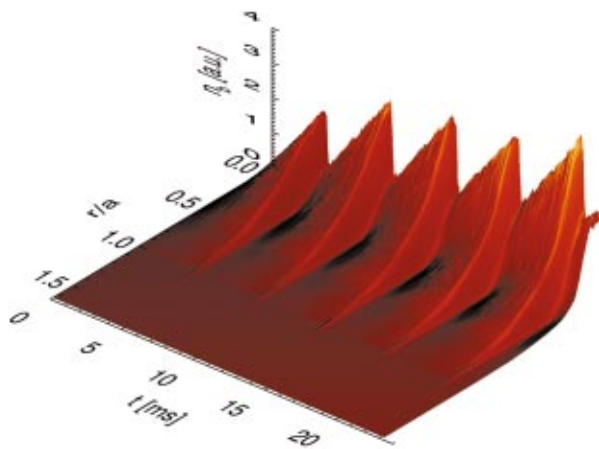FIG. 22. (Color) Plot of time evolution of the beam ion density in (t,r) space for counter-injection.

D. Effects of beam injection direction

We have observed a complete contrast in the capacity to store beam energy between co- and counter-injected beam ions when TAE excitations are present. Compared to the classical transport predictions for the parameters of the simulation, about 2/3 of the classically predicted co-beam energy was stored, while only about 0.1 of the classically predicted counter-beam energy was stored. To better understand this difference it is interesting to investigate separately the time evolutions of purely co- and purely counter-injection.

First we examine purely counter-injection. In this run only the counter-beam is injected with a heating power of 10 MW. All other conditions are the same. The time evolution of the mode amplitude is shown in Fig. 20. The saturation amplitude of modes 1 and 3 exceed $\delta B/B \sim 3 \times 10^{-2}$ while that of mode 2 and 5, that were dominant in the balanced-injection run, are at lower levels. Figure 21 shows the time evolution of stored beam energy. The modulation depth of the drop in the stored beam energy is 83%, which is larger than that of the counter beam particles in the balanced injection run ~50%. In the relative units of this figure, the classical stored energetic particle distribution of counter injected
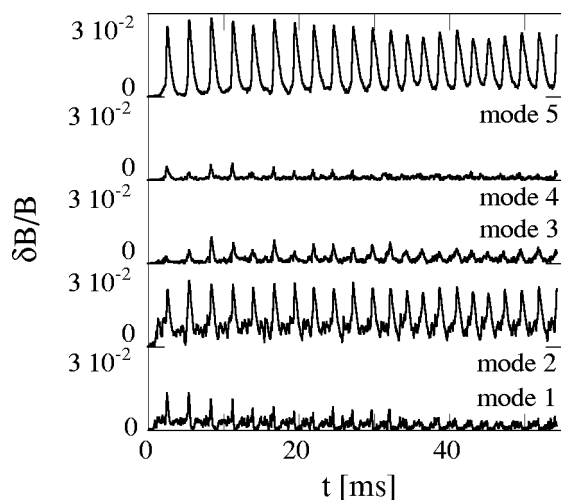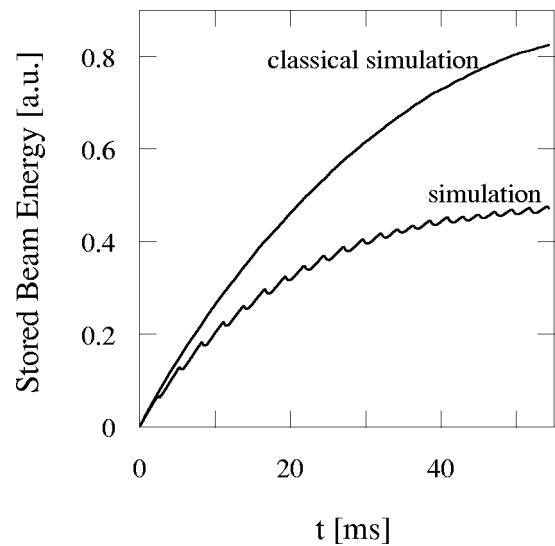

FIG. 24. Time evolution of stored beam energy using only co-injected beams. Result from simulation is compared with the classical result.

particles saturates at a relative level of 0.74 which is twice that of the classically stored counter-injected beam energy shown in Fig. 3. In contrast the stored energy of the simulation saturates at a peak relative level of 0.11, namely, 15% of that of the classical simulation. The time interval of the bursts is about 4.4 ms which is about 1.5 the burst period of the balanced-injection run. It takes a longer time for the beam ion distribution to build up to a level to excite a burst, because more than 80% of the beam energy is lost at each burst and the total increase in stored energy, starting from the minimum stored energy state, is more than in the previous run, when there was a smaller change of stored energy between each burst. Figure 22 shows a plot of the time evolution of the counter-injected beam ion density as a function of the minor radius r after it is averaged in the poloidal and toroidal directions. Clearly the changes in beam ion density associated with TAE bursts are large.

Next we investigate purely co-injection. What is changed from the previous runs is that only the co-beam is
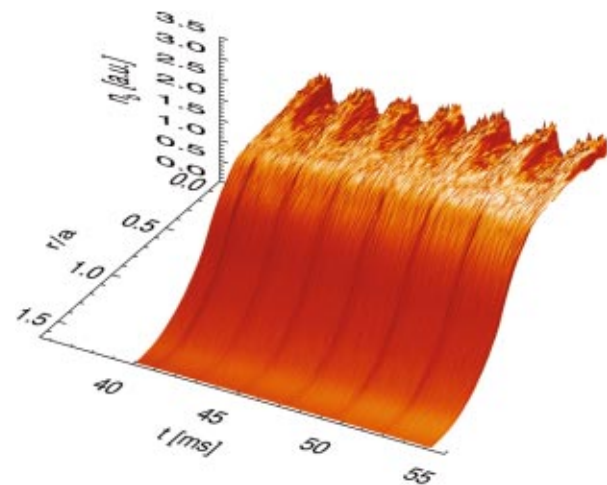

FIG. 23. Amplitude evolution for all the eigenmodes for co-injected beams.

FIG. 25. (Color) Plot of time evolution of the beam ion density in (t,r) space after $t=40$ ms with co-injected beams.

injected with the heating power of 10 MW. The time evolution of the mode amplitudes are shown in Fig. 23. The saturation amplitudes of the dominant two modes, 2 and 5, are the same as in the balanced-injection run. Figure 24 shows the time evolution of stored beam energy. The modulation depth of the drop in the stored beam energy is 3% which is comparable to the fractional drop of the co-injected beam (3%) in the balanced run. In the relative units of this figure, the ideal classical stored energetic particle distribution saturates at relative level of 0.83, whereas that of the simulation roughly saturates at a relative level of 0.48, namely, 58% of that of the ideal classical simulation. The period between bursts is about 2.5 ms which is substantially shorter than the counter-injection run and a slightly shorter period than with balanced injection. Figure 25 shows a plot of the time evolution of the co-injected beam ion density as a function of the minor radius r after it is averaged in the poloidal and toroidal directions. In a manner similar to Fig. 8(b), the density gradient in the plasma center take place at each burst, while the change of particle number at the plasma edge is small. In the next section we discuss whether the edge gradient affects the stability.

E. Effects of the edge gradient on the stability

In order to investigate the effect of the edge gradient on the stability we have carried out another run which modifies the purely co-injection run, starting at a time when the profile is flattened in the core ($t = 50.1$ ms). We attempt to minimize the effect of instability arising from the core pressure gradient by modifying the simulation just at a time that the internal core pressure gradient is flattened by a TAE burst. Due to the intrinsic mode damping finite pressure gradient remains at this moment although the mode amplitudes are decreasing in Fig. 23. We have confirmed that the density profile is completely flattened in the core ($r/a \leqslant 0.72$) at this moment. The run is restarted at this moment with the beam ion pressure doubled everywhere, thereby increasing the edge pressure gradient. In addition beam injection and collisions are turned off. Figure 26 shows the time evolution of the dominant two modes 2 and 5, and beta value at various minor radii. We see that the mode amplitudes initially slightly grow due to the doubled pressure and eventually damp to low levels $\delta B/B \sim 10^{-3}$. The pressure profile settles to a steady state which appears to be marginally stable. We should notice that even the doubled pressure profile at the edge ($r/a \geqslant 0.72$) is maintained. This suggests that the original edge gradient, which is maintained by particles sticking out of the plasma, has only negligible effects on wave stability. We can infer that in our usual runs that the stability is governed by newly injected particles since there are regularly repetitive bursts that appear with the same time intervals, amplitudes, and particle loss. These characteristics apply to runs with, balanced-injection, purely counter-injection, and purely co-injection. In these runs, the newly injected particles cause the internal particle profile to peak at the plasma center and this gradient drives the instability that flattens the internal profiles that the newly injected particle have built up. In addition there is loss of part of the ion population. Newly injected
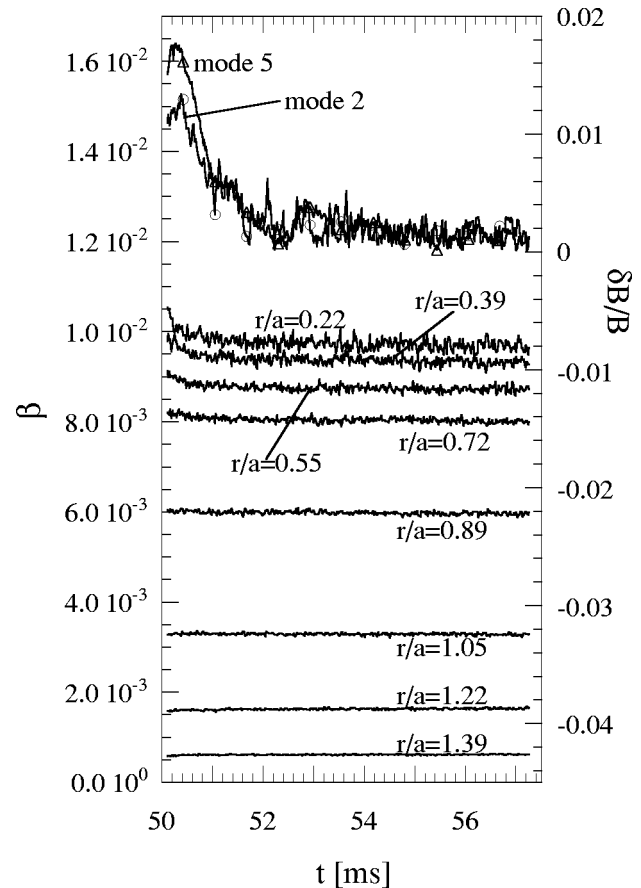

FIG. 26. Time evolution of the dominant two modes 2 and 5 and the beta value of the co-injected beam ions at various minor radii in the run which succeeds the purely co-injection run, starting at a time when the profile is flattened in the core ($t = 50.1$ ms). When the run is started the beam ion pressure is doubled.

co-passing particles which are not lost by their first burst are scattered to the plasma edge. Co-passing particles at the plasma edge can survive the subsequent bursts because the interaction between the particles and the TAEs is weak and there is a enough space between the plasma edge and the limiter. They stay at the plasma edge for a long time comparable to the slowing down time and form a pedestal which support the spatial profile in the core. On the other hand counter-passing particles do not have such a space to stay and they are lost after one or two bursts.

IV. DISCUSSION AND SUMMARY

Our simulation of the energetic particle interaction with a selected set of TAE modes predicts saturation levels of $\delta B/B \sim 2 \times 10^{-2}$. The experimental amplitude measured by Mirnov coils at the plasma edge is $\delta B/B \sim 3 \times 10^{-5}$,[15] much lower than simulation predicts. However, we cannot compare the simulation amplitude with that measured by Mirnov coils because the structure of the eigenfunction is not accurate near the edge because the MHD description is not valid in the vacuum gap. On the other hand, the experimental plasma displacement has been estimated $\xi \sim 5 - 10$ mm from the density fluctuation.[16] This enables us to estimate the amplitude $\delta B/B \sim v/V_A \sim \omega \xi / \omega_A R \sim 0.6 - 1.3 \times 10^{-3}$. With this esti-

mate there remains a discrepancy of one order of magnitude with the results of our simulation. Other nonlinear mechanisms, that have not considered in this study, might suppress the level of mode amplitudes observed in this simulation and yet still produce fast energetic particle diffusion at perturbed field levels that are closer to what experiment would estimate. One possible mechanism that could reduce the mode level without changing the magnitude of the particle bursts is MHD mode coupling to a broader spectrum of waves. More sophisticated MHD calculations are needed to examine how lower level saturation can be achieved. Still it is quite conceivable that the rate and magnitude of energetic particle loss observed in both experiment and in this simulation are relatively insensitive to the peak amplitude, but dependent on the self-consistent energetic particle pressure profile that will induce global stochasticity.

Bursting behavior of TAEs has been described using the heuristic predator-prey model[17] and our simulation captures some aspects of this model and gives a physical mechanism for the predator–prey response. It has been previously argued that resonance overlap synchronizes the behavior of multiple TAEs and can explain the experimentally observed intermittent TAE bursts and energetic particle loss (see Ref. 5 which used a reduced simulation and Refs. 18, 19 which are based on quasilinear models). In this paper we have made the first numerical demonstration, using parameters that are quite similar to that of experiment, that a numerical simulation can closely reproduce many experimental characteristics. These include: (a) the synchronization of multiple TAEs taking place at time intervals fairly close to the experimental value; (b) the modulation depth of the drop in the stored beam energy that closely matches the experimental value; (c) the stored beam energy saturating at about one-half to one-third of that predicted for a classical slowing down distribution. We have analyzed the particle loss mechanism and found particle loss that is due to: (1) the resonance overlap of different eigenmodes; (2) the disappearance of KAM surfaces in phase space due to overlap of multiple nonlinear islands created by a single eigenmode. We have found that counter-injected beam ions are much more easily lost than co-injected passing particles when the limiter is such as to preferably scrape-off particles whose equilibrium orbits are shifted to the inside of the toroidal boundary. The surviving counter-injected particles are sharply peaked in the center. In contrast, the co-injected beam ions have difficulty reaching the limiter because their equilibrium orbits are shifted to the outside of the torus where there is a great deal of room between the plasma edge and the limiter. As a result a co-moving particle tends to survive diffusion to the edge and it is likely to diffuse back to the inside of the plasma. Their stored energy profile is extended throughout the confinement region, and quite significantly, their population can be built up to a substantial fraction of the classical level! For the purely counter-injected beam, a large fraction of the stored beam ions is lost with each burst, even when the stored energy is quite low and we observe longer burst intervals than in either the balanced or co-injected cases. This is because there is a larger change of stored energy between bursts, even though the maximum stored energy is substantially lower

than in the other two cases. For the purely co-injected beam we have found that modest gradients in the center are periodically flattened but the edge gradient near the wall can become large. Remarkably, this gradient appears to have a negligible effect on wave stability.

In summary, except for the saturation of the field level, our simulations appear to match the TFTR experiment.[2,4] We reproduce the saturated stored energy, the burst rate and the magnitude of particle loss per pulse. This achievement suggests that the loss characteristics are insensitive to the specific nonlinear mechanisms that truly exist in the experiment. The identification of the true mechanism of wave saturation and particle loss remains to be identified in future work. Furthermore, we have concluded that the stored beam energy should be predominantly in the co-direction when there is a limiter leaning on the inner edge. It would be interesting to verify this assertion in future experiments, as past data regarding this issue does not appear to be available.

Since successful confinement of energetic alpha particles is required for self-sustained operation, the nonlinear evolution of TAEs, especially the TAE bursts, is an important issue for fusion plasmas. We have demonstrated that reduced simulations, like the one presented here, may be extremely useful in the future in predicting the characteristic response of alpha particles in burning plasma regimes when TAE modes are excited.

ACKNOWLEDGMENTS

[1] C. Z. Cheng and M. S. Chance, Phys. Fluids **29**, 3659 (1986).
[2] K. L. Wong, R. J. Fonck, S. F. Paul et al., Phys. Rev. Lett. **66**, 1874 (1991).
[3] W. W. Heidbrink, E. J. Strait, E. Doyle, G. Sager, and R. T. Snider, Nucl. Fusion **31**, 1635 (1991).
[4] K. L. Wong, R. Durst, R. J. Fonck et al., Phys. Fluids B **4**, 2122 (1992).
[5] H. L. Berk, B. N. Breizman, and M. S. Pekker, Nucl. Fusion **35**, 1713 (1995).
[6] J. Candy, H. L. Berk, B. N. Breizman, and F. Porcelli, Phys. Plasmas **6**, 1822 (1999).
[7] Y. Todo, T.-H. Watanabe, H.-B. Park, and T. Sato, Nucl. Fusion **41**, 1153 (2001).
[8] R. J. Goldston and P. H. Rutherford, *Introduction to Plasma Physics* (Institute for Physics, Bristol, 1995).
[9] A. H. Boozer and G. Kuo-Petravic, Phys. Fluids **24**, 851 (1981).
[10] Y. Chen, R. B. White, G. Y. Fu, and R. Nazikian, Phys. Plasmas **6**, 226 (1999).
[11] R. Nazikian, G. Y. Fu, S. H. Batha et al., Phys. Rev. Lett. **78**, 2976 (1997).
[12] G. Y. Fu and J. W. Van Dam, Phys. Fluids B **1**, 1949 (1989).

[13] G. Y. Fu, R. Nazikian, R. Budny, and Z. Chang, Phys. Plasmas **5**, 4284 (1998).

[14] S. E. Parker and W. W. Lee, Phys. Fluids B **5**, 77 (1993).

[15] D. S. Darrow and Theory Groups, Bull. Am. Phys. Soc. **44**, 364 (1999).

[16] R. D. Durst, R. J. Fonck, K. L. Wong, C. Z. Cheng, E. D. Fredrickson, and S. F. Paul, Phys. Fluids B **4**, 3707 (1992).

[17] W. W. Heidbrink, H. H. Duong, J. Manson, E. Wilfrid, C. Oberman, and E. J. Strait, Phys. Fluids B **5**, 2176 (1993).

[18] H. L. Berk, B. N. Breizman, J. Fitzpatrick, and H. V. Wong, Nucl. Fusion **35**, 1661 (1995).

[19] H. L. Berk and B. N. Breizman, in *Theory of Fusion Plasmas, 1998*, Varenna (Società Italiana di Fisica, Bologna, 1999), p. 283.